Bioresource Technology 178 (2015) 19–27

Contents lists available at ScienceDirect

Bioresource Technology

journal homepage: www.elsevier.com/locate/biortech

Heterogeneous catalyst-assisted thermochemical conversion of food waste biomass into 5-hydroxymethylfurfural

Ganesh K. Parshetti, Maria Stefanie Suryadharma, Thi Phuong Thuy Pham, Russell Mahmood, Rajasekhar Balasubramanian *

Department of Civil and Environmental Engineering, National University of Singapore, 1 Engineering Drive 2, Singapore 117576, Republic of Singapore

HIGHLIGHTS

- A novel thermochemical system was developed for conversion of food waste to HMF.
- The catalyst (ZrP) was characterized by SEM, XRD, XPS, BET and NH3-TDP.
- The optimized reaction conditions were developed to maximize HMF yield.
- Catalysts were easily regenerated by thermal treatment and can be used for 3 cycles.
- "Minimum selling price" of HMF found to be significantly lower than market price.

GRAPHICAL ABSTRACT

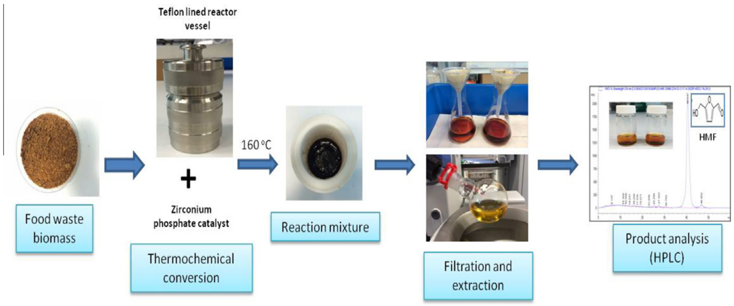
Teflon lined reactor vessel
Food waste biomass
+
Zirconium phosphate catalyst
Thermochemical conversion
160 °C
Reaction mixture
Filtration and extraction
HMF
Product analysis (HPLC)

ARTICLE INFO

Article history:
Received 30 July 2014
Received in revised form 11 October 2014
Accepted 13 October 2014
Available online 18 October 2014

Keywords:
Thermochemical conversion
Food waste biomass
5-Hydroxylmethylfurfural
Zirconium phosphate
NH_3-TPD

ABSTRACT

A novel thermochemical conversion route has been developed that yields 5-hydroxymethylfurfural (HMF) from food waste biomass (FWB) in the presence of a heterogeneous catalysts (zirconium phosphate (ZrP)). The ZrP catalyst was prepared by precipitation followed by calcination at 400 (ZrP-400) and 600 °C (ZrP-600) and was characterized by SEM, XRD, XPS, N_2 sorption and NH_3-TPD. The optimized reaction conditions were identified to maximize HMF yield by varying the type of catalyst, the catalyst loading and the reaction time. The highest HMF yield achieved was 4.3%. On average 33% higher yield for ZrP-600 was obtained compared to that for ZrP-400, which might be due to higher number of acid sites on ZrP-600. The ZrP catalyst was easily regenerated by thermal treatment and showed stable activity upon its reuse. Preliminary calculations of the "minimum selling price" of HMF suggest that it is economically attractive to make this industrially-relevant chemical from FWB.

© 2014 Elsevier Ltd. All rights reserved.

1. Introduction

There has been considerable recent interest in the production of chemicals and liquid fuels from biomass (Corma et al., 2007; Sheldon 2014). Among the many possible biomass-derived chemicals, 5-hydroxymethylfurfural (HMF) prepared from the dehydration of carbohydrates is considered to be a key bio-based platform compound, as it is versatile and a key intermediate in the production of biofuels, pharmaceuticals and fine chemicals. HMF derivatives also can be used as ingredients in the polymer, food and agricultural industries (Xiao et al., 2014). However, the current processes of HMF production are primarily dependent on edible conversion feedstocks such as monosaccharides and disaccharides (fructose, sucrose and glucose), whose continued use may have a negative impact on the global food supplies. The need to find new renewable resources has led to exploring the use of food supply chain waste (FSCW) as a renewable biorefinery

---

* Corresponding author. Tel.: +65 65165135; fax: +65 67744202.
E-mail address: ceerbala@nus.edu.sg (R. Balasubramanian).

http://dx.doi.org/10.1016/j.biortech.2014.10.066
0960-8524/© 2014 Elsevier Ltd. All rights reserved.

feedstock; FSCW refers to “the organic (biomass) material produced for human consumption discarded, lost or degraded primarily at the manufacturing and retail stages” (Lin et al., 2013). Vast amounts of food waste (FW) is generated and discarded in countries with high population densities (Pfaltzgraff et al., 2013). For example, a recent report by the Singapore National Environmental Agency (NEA) indicated that the amount of FW generated in Singapore (population of about 5.2 million) hit a record high of 703,200 tons in 2012 (Parshetti et al., 2014). In recent years, there is a strong impetus to develop a viable technology for conversion of food waste biomass (FWB) to value-added chemicals such as HMF (Pfaltzgraff et al., 2013).

Various reaction media including organic solvent/organic-water biphasic systems, ionic liquids and the aqueous phase were used for HMF production (Dashtban et al., 2014). However, organic solvent and ionic liquid reaction media pose economic and environmental limitations for the large scale production of HMF. The use of aqueous phase (i.e. water) instead of these expensive and difficult-to-separate solvents would significantly reduce its production cost. In addition, the aqueous medium possesses several practical advantages such as efficient processing of recalcitrant feedstocks under sub- or super-critical conditions, high solubility with chemicals and lack of media toxicity unlike organic solvents. Among several aqueous methods, the hydrothermal treatment (HT) is one of thermochemical methods that have generated a widespread interest in recent years for conversion of biomass to fuels and chemicals (Brown, 2011). HT, also known as the wet torrefaction in the subcritical region (100–374 °C), has been considered as a cost-effective pretreatment method with limited equipment corrosion and simple operation with minimal technical training (Chang et al., 2013). A key advantage of HT is that even wet feedstocks or raw materials with high moisture contents can be directly processed and it could accelerate the formation of HMF from carbohydrates and sugars (Aida et al., 2007; Kuster, 1990).

However, the degradation of saccharides (e.g. fructose and glucose) in water-only conditions proceeds with poor selectivity to HMF production, resulting in many by-products. By-products such as glycolaldehyde, glyceraldehyde and lactic acid could be co-produced with HMF from glucose and fructose, while other chemicals such as levulinic acid and formic acid could result from the rehydration of HMF, affecting the overall yield of the desired product, HMF (Aida et al., 2007). Therefore, the use of catalysts has been suggested for HMF production in aqueous environments with high selectivity; the promising catalysts include mineral acids (e.g. H_2SO_4, H_3PO_4, and HCl), organic acids (e.g. oxalic acid, ρ-toluenesulfonic acid), H-form zeolites, strong acid cation exchange resins, and solid metal phosphates (Yan et al., 2013). These catalysts can assist the isomerization of glucose to fructose, which is a key step for HMF production (Yan et al., 2013). However, mineral and organic acids could also accelerate the rehydration of HMF, thereby limiting its yield (Asghari and Yoshida, 2006). On the other hand, H-form zeolites, strong acid cation exchange resins are often not suitable to catalyze the conversion of water-insoluble polysaccharides (e.g. cellulose) into degradation products (e.g. HMF) due to mass transfer limitation (Huang and Fu, 2013). In recent years, heterogeneous catalysts such as Zirconium phosphate (ZrP) were shown to be effective for transforming saccharides into HMF. ZrP is also an important solid acid catalyst with high thermal stability, high water tolerance ability and easy sedimentation, allowing its possible recovery and reuse (Ordomsky et al., 2013). Carlini et al. (2004) and Benvenuti et al. (2000) reported the good performances of metallic phosphates, which are generally considered as weak Brønsted/Lewis acids, for HMF synthesis. In the present study, a novel route for producing HMF from FWB using ZrP-assisted hydrothermal technology was explored. The reaction conditions were optimized to maximize the HMF yield. The pathway involved in the conversion of FWB to HMF is also discussed. Further, proposed a conceptual plant design to estimate the cost of production of HMF and compared this cost with the current market price.

2. Methods

2.1. Materials

FW was collected from a major multi-ethnic food outlet at the National University of Singapore. Visual observation of the FW indicated that the waste consisted of a variety of cooked food (e.g., chicken, seafood, potato fries, vegetables, leftovers like rice and gravy), uncooked food (e.g., fruit peels, vegetable parts) and condiments (e.g., salad dressing, ketchup, cocktail sauce). The collected waste was weighed and immediately separated out for bones, eggshells, plastic utensils, etc. because of processing limitations. Following separation, the FWB was mixed and homogenized with a food grade blender and stored at 4 °C prior. Di-ammonium hydrogen phosphate ($(NH_4)_2HPO_4$, ACS Reagent, for analysis) and zyrconyl chloride octahydrate ($ZrOCl_2{\cdot}8H_2O$, for analysis) were purchased from Merck for catalyst synthesis. Ethyl acetate (ACS Reagent, ⩾99.5%), and standard 5-hydroxymethyl furfural (99%) were purchased from Sigma–Aldrich.

2.2. Characterization of FWB

Ultimate elemental (CHNS) analysis was done using an elemental analyser (Vario Macro Cube, Elementar, Germany). Total solid (TS) and moisture content tests were done using the following procedures: wet mass of FW (m_W) was recorded before it was heated to dryness at 103 °C for 2 h. The dried FWB was weighed, and was further heated for 30 min followed by another weighing. This procedure was repeated until the change in mass was less than 4%, and the final mass was recorded (m_{TS}). Volatile solid (VS) test was done by heating the dried FWB in a muffle furnace at 550 °C for 2 h. Similarly, the procedure was repeated until the change in mass was less than 4%, and the final mass was recorded (m_{FS}). The total solid and volatile solid contents were calculated as follows:

$$\%TS = \frac{m_{TS}}{m_W} \times 100\% \tag{1}$$

$$\%VS = \frac{m_{TS} - m_{FS}}{m_{TS}} \times 100\% \tag{2}$$

$$\text{Moisture content} = 100\% - \%TS \tag{3}$$

The concentration of trace elements in FWB was determined using ICP-OES (Perkin Elmer, ELAN 6100, USA) analysis. A multi-elemental standard was used for calibration of the ICP-OES. Metal concentrations are expressed as micrograms per gram of sample ($\mu g\ g^{-1}$).

2.3. Catalyst synthesis

ZrP was prepared using the following experimental procedure, which consisted of precipitation of $(NH_4)_2HPO_4$ (1 M, 200 ml) and $ZrCl_2O{\cdot}8H_2O$ (1 M, 100 ml) at a molar ratio of P/Zr = 2. The solution was stirred at the room temperature and then filtered, washed with de-ionized (DI) water until pH 5 and dried overnight at 100 °C. The dried powder was calcined at a constant heating rate of 5 °C min^{-1} at 400 and 600 °C and held at these temperatures for 3 h. The ZrP catalyst thus produced is referred to as ZrP-400 and ZrP-600, in accordance with the calcination temperature (i.e. 400 °C or 600 °C).

2.4. Catalyst characterization

The surface morphology of the materials was examined by scanning electron microscopy (SEM) (JEOL JSM-6700F Oxford Inca Energy 400), operated at an electron accelerating voltage of 15 kV. Prior to scanning, the samples were kept onto carbon adhesive tape on an aluminum stub and coated with a thin layer of gold under high vacuum (10^{-3} to 10^{-7} mbar) conditions using an Ion Sputter E-1030 (Hitachi, Japan). Wide angle X-ray diffraction (XRD) patterns were recorded on a Bruker D8 ADVANCE (Germany) X-ray diffractometer equipped with Ni-filtered Cu Kα radiation (k = 1.5406 Å) operating at 40 kV and 40 mA. The diffraction patterns were collected over a 2θ range of 5–70°. X-ray Photoelectron Spectroscopy (XPS) analysis of the materials was carried out using a VG ESCA 220i-XL Imaging (Thermo VG Scientific Ltd., UK). Monochromatic Al Kα X-ray ($h\nu$ = 1486.6 eV) was employed for analysis with photoelectron take-off angle of 90° to the surface plane. The analysis area was approximately 700 mm in diameter while the maximum analysis depth was in the range of 4–8 nm. Survey spectra were acquired for elemental identification while high-resolution spectra were acquired for chemical state identification. For chemical state analysis, a spectral deconvolution was performed by a curve-fitting procedure based on Lorentzians broadened by a Gaussian function using the manufacturer's standard software. The error in binding energy measurements was estimated to be within ±0.2 eV. The textural properties of materials were characterized by N_2 adsorption at 77 K in a gas adsorption instrument (The *Micromeritics* ASAP 2010 (Accelerated Surface Area and Porosimetry System)). Prior to each measurement, the material was outgassed at 180 °C for 2 h in vacuum to clean its surface. Specific surface areas were calculated with the Brunauer–Emmett–Teller (BET) equation from N_2 adsorption data. Total pore volume was calculated from the amount of nitrogen adsorbed at $P/P_0 = 0.99$. The acidic properties were studied by temperature-programmed desorption of ammonia (NH_3-TPD). Prior to adsorption, the samples were pretreated in a flow of dry air at 600 °C for 1 h and, subsequently, in a flow of dry helium for 1 h and cooled down to ambient temperature. For NH_3 adsorption, a sample was subjected to a flow of diluted NH_3 for 15 min. The physisorbed NH_3 was removed in a flow of dry helium at 100 °C for 1 h. Typical TPD experiments were carried out in the temperature range of 80–600 °C in a flow of dry helium. The rate of heating was 10 °C min^{-1}. The desorbed NH_3 was analyzed by a thermal conductivity detector (TCD) detector.

2.5. Thermochemical conversion of FWB and product characterization

Prior to thermochemical conversion, FWB was dried completely and ground into powder form. Drying is not necessary for the reaction itself, but to eliminate the effect of varying moisture content and ensure accuracy. The same batch of FWB was used throughout the experiment to ensure homogeneity. Batch reactions were carried out in a 100 mL a Teflon®-lined high pressure reactor vessel provided by Latech Scientific Supply Pte. Ltd. The dried FWB (4 wt%) and ZrP catalysts (1 wt% and 2 wt%) were mixed with distilled water in a reactor and kept in a heating oven (Binder, FD53) at 160 °C temperature for the desired time duration (2–6 h). The temperature of the oven was set to increase at 5 °C min^{-1}, and the reaction time was counted from the moment the oven reached the desired temperature. After reaction time, the reactor was cooled and the resulting reaction mixtures were filtered. The filtrate was mixed with ethyl acetate in 1:1 volume ratio in a separating funnel to extract HMF using rotary evaporator (IKA RV 10) at 45 °C and 120 rpm. HMF standard solutions and exaction products were analyzed by high-pressure liquid chromatography (HPLC) with a 1200 HPLC system coupled with a UV–Vis Detector (G1314B). The column used was a Biorad Aminex HPX-87H sugar column, and the mobile phase was 0.005 M H_2SO_4 with a flow rate of 0.6 ml min^{-1}. HMF yield was calculated using following equation:

$$\text{Yield (wt\%)} = \frac{\text{amount of HMF (g)}}{\text{initial amount of FWB (g)}} \times 100\% \qquad (4)$$

3. Results and discussion

3.1. FWB characterization

For this preliminary study, the FW collected from Singapore was considered as it has a multi-cultural society consisting of 74% Chinese, 13% ethnic Malay, 9% Indian, and 3% Eurasian. The details chemical compositions of FWB are given in Table S1 (see supplementary information). The initial chemical composition of the FWB is provided because the diets from different regions around the world are very different so the applicable scope of the results from this research can be defined by the composition of FWs. The FWB used in the study had 80.2% moisture, 16–19% total solids and 94.3% volatile solids. The results of the CHNS analysis showed that the FWB contained C (45.5 wt%) and O (44.6 wt%) as their most important components followed by hydrogen (7 wt%), nitrogen (2.4 wt%) and sulfur (<0.5 wt%). Further. FWB contained only trace amounts of inorganic elements (Table S1, see supplementary information). Thus it is clear that the FWB used in the present study had a high content of organics that were composed of carbohydrate, protein, lipid and fibers.

3.2. ZrP characterization

Morphology of the ZrP catalyst was investigated by SEM. As shown in the SEM micrographs (Fig. S1a and b, see supplementary information), the ZrP powder clearly showed a plate-like and irregular particles resulting from dispersion and aggregation of ZrP suggesting its semi crystalline nature. The particles are on average a few hundred nanometers wide and some tens of nanometers thick, and are connected so as to form irregular pores with a size on the micron scale. The structural composition of the ZrP materials was examined using XRD. The XRD patterns of the ZrP samples prepared at 400 and 600 °C are shown in Fig. S2 (see supplementary information). No individual crystalline peak of ZrP and zirconia was observed in the samples calcined at both temperatures. In the wide angle XRD patterns, two broad peaks in 2θ range of 10–40° and 40–70° indicated the amorphous nature of the synthesized ZrP samples, which is attributable to layered zirconium pyrophosphate and very likely to semi-crystalline anhydrous zirconium hydrogen phosphate (Bellezza et al., 2006).

XPS measurements of the ZrP materials were performed to gain information about their composition. Fig. S3, (see supplementary information) shows the high resolution XPS spectra of zirconium, phosphorus, and oxygen for the both zirconium phosphate catalysts. The Zr3d line is composed of two major peaks assigned to Zr3d5/2 at 183 eV and Zr3d3/2 at roughly 185.8 eV. This is characteristic of tetravalent zirconium (Zr^{4+}) (Yuan et al., 2005). Both materials had typical P2p binding energies of 133 eV, characteristic of pentavalent tetracoordinated phosphorus (P^{5+}) (Yuan et al., 2005; Puziy et al., 2006). The O1s line shows a broad peak which could correspond to oxygen atoms bonded to both zirconium and phosphorus (Yuan et al., 2005). The surface atomic compositions of the zirconium and phosphate appear in Table 1. These values were determined by the XPS line areas of Zr3d and P2p and the zirconium to phosphorus atomic ratios on the surface were calculated accordingly and the compounds examined shows expected Zr:P

Table 1
Atomic composition of P and Zr in ZrP-400 and ZrP-600 based on XPS peaks.

Element	ZrP-400		ZrP-600	
	Peak BE (eV)	Atomic%	Peak BE (eV)	Atomic%
P	134.0	67.8	134.3	69.7
Zr	183.5	32.2	183.7	30.3

ratio of 1:2. This value indicates the presence of strongly absorbed phosphoric acid, or the presence of some dihydrogen phosphate groups together with the monohydrogen phosphate groups (Weingarten et al., 2013).

Fig. 1a and b show the nitrogen adsorption–desorption isotherms of the ZrP-400 and ZrP-600 catalysts at 77 K, respectively. The isotherms can be classified as type IV, with pronounced adsorption–desorption hysteresis which confirms that the mesopores are fairly irregular. Fig. 1c and d show the pore size distribution curves determined from the adsorption branches of the isotherms. The pore size distributions, calculated using the BJH formula, show the maximum peaks in the mesopore range. The surface areas (BET) and pore volumes as well as average pore diameters (BJH adsorption) for the materials are listed in Table 2. A clear difference in surface areas and pore volumes between samples ZrP-400 and ZrP-600 is observed. ZrP-400 catalysts possesses a specific surface area (BET) of 35.09 $m^2\,g^{-1}$, pore volume of 0.149 $cm^3\,g^{-1}$ and average pore diameter of 17.03 nm while the sample ZrP-600 has a specific surface area (BET) of 46.40 $m^2\,g^{-1}$, pore volume of 0.179 $cm^3\,g^{-1}$ and average pore diameter of 15.49 nm.

NH_3-TPD was measured to evaluate the total acidity and the strength of acid sites of the synthesized ZrP. There was a broad desorption profile over the range 100–550 °C in the NH_3-TPD profiles (Fig. S4, see supplementary information), suggesting a wide distribution of heterogeneous acid sites existing on the solid acid surface. The amounts of acid sites on ZrP-400 and ZrP-600 were 612 and 750 μmol g^{-1}, respectively (Table 2). The high value of the acid on the ZrP-600 may be due to its high surface area (46.40 $m^2\,g^{-1}$) as compared to ZrP-400 (35.09 $m^2\,g^{-1}$). Only one peak (around 200 °C) on the NH_3-TPD spectrum for ZrP-400 and ZrP-600 (Fig. S4, see supplementary information) suggests weak acid sites on the surface of these catalysts (Watanabe et al., 2005).

3.3. Optimization of HMF yield and pathway

HMF can be obtained from carbohydrates contained in FWB. Preliminary experiments on the HMF production were carried out with and without ZrP in order to understand the role and effectiveness of the catalyst as shown in Fig. S5 (see supplementary information). It was found that the conversion of FWB can proceed with or without the catalyst, but the usage of ZrP effectively promoted a faster and favorable reaction rate from the conversion of FWB to HMF viewpoint. For instance, at a reaction time at 6 h, the HMF yields catalyzed by 1 wt% ZrP-400 and ZrP-600 (2.1% and 2.9%, respectively) were higher than without catalyst (0.9%) (Fig. S5, see supplementary information). Further, the effect of ZrP calcination temperature on HMF was evaluated, and the results show that calcination temperature was observed to have significant effects on the catalyst performance. On average 33% higher HMF yield for ZrP-600 was observed compared to ZrP-400 (Data not shown). This can be explained by the fact that the catalyst upon calcination at 600 °C had larger surface area and more acid sites which caused the hydrolysis and dehydration to occur smoothly (Table 2) (Carlini et al., 2004; Yang et al., 2011a,b; Weingarten et al., 2013).

The influence of the catalyst dosage and the reaction time with respect to FWB conversion into HMF was investigated. The effect of catalyst (ZrP-400 and ZrP-600) dosage was studied at 1 and 2 wt% concentration and effect of reaction time was studied by varying the duration from 2 to 6 h as shown in Fig. 2. The results showed that the more the catalyst loading, the higher the HMF yield, which might be attributed to an increase in the availability and number of catalytically active sites (Carlini et al., 2004; Yang et al., 2011a,b; Ordomsky et al., 2013). It was also noted that the reaction time exhibits great influence on HMF yield and conversion efficiency. As shown in Fig. 2, the conversion of FWB increased sharply with the reaction time ranging from 2 to 6 h. In case of 2 wt% of

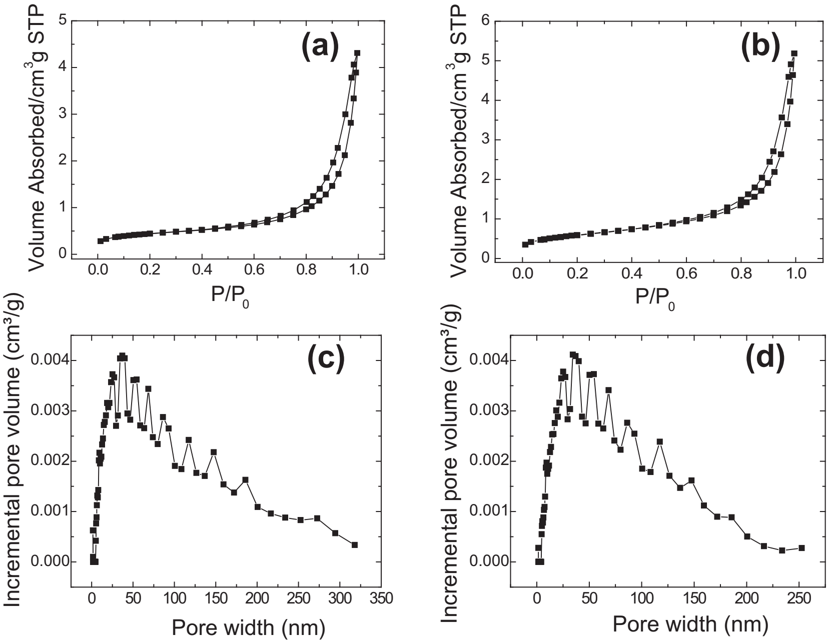

Fig. 1. (a) N_2 adsorption–desorption isotherms of ZrP-400 at 77 K. (b) N_2 adsorption–desorption isotherms of ZrP-600 at 77 K. (c) Pore size distribution (PSD) of ZrP-400. (d) Pore size distribution (PSD) of ZrP-600.

Table 2
Characterization of ZrP-400 and ZrP-600 catalysts by BET and NH_3-TPD studies.

	S_{BET} (m^2 g^{-1})[a]	V_{total} (cm^3 g^{-1})[b]	D_p (nm)[c]	Total acid sites (μmol g^{-1})[d]
ZrP-400	35.09	0.149	17.03	612
ZrP-600	46.40	0.179	15.49	750

[a] Specific surface area determined by the BET method for P/P_0 between 0.05 and 0.3.
[b] Total pore volume calculated at $P/P_0 = 0.99$.
[c] Average pore diameter.
[d] Determined from NH3-TPD.

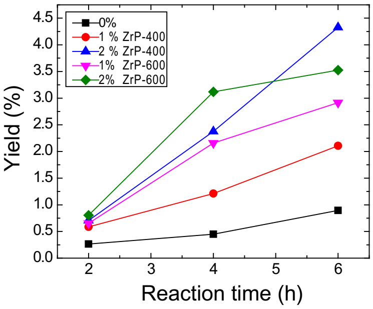

Fig. 2. Effect of reaction time and catalyst concentration on HMF yield.

ZrP-400 and ZrP-600, the HMF yield increased from 0.7% to 4.3% and 0.8% to 3.5% respectively when the reaction time was increased from 2 to 6 h. As for 1 wt% of ZrP-400 and ZrP-600, the HMF yield increased from 0.5% to 2.1% and 0.6% to 2.9%, respectively. Thus, a higher yield of HMF can be achieved at 6 h for both ZrP-400 and ZrP-600 at different catalyst concentrations.

The maximum yield of HMF was 4.3%, obtained using 2 wt% ZrP-400 at 160 °C reaction temperature and 6 h reaction time (Table 3). Some studies reported a 5% to 7% yield of HMF where chloride ionic liquid and acid catalysts were used for the conversion of cellulose to HMF Binder and Raines (2010). Compared to the some of the published studies which used the various catalysts such as ZrP, zirconium dioxide, Anastase TiO_2, γ-Al_2O_3 and niobium pentoxide for HMF conversion from biomass (Watanabe et al., 2005; Yan et al., 2013, Weingarten et al., 2011, 2013; Ordomsky et al., 2013), the maximum yield obtained in this study is rather lower. The main reason for the lower yield is that previous studies used pure glucose or carbohydrate precursors as starting materials, while FWB in this study contains complex carbohydrates along with protein and lipid polymers, which require more energy to break down. Secondly, the heterogeneous reaction over solid acid catalysts generally suffers from low catalytic activity due to the solid-solid contact between the insoluble FWB macromolecules/polymers (lipids and proteins) and solid catalyst (Lin et al., 2012). However the minimum selling price of HMF produced using current thermochemical process is significantly lower compared to the current market price; this is discussed in a later section (Conceptual design and economic analysis) of this manuscript.

Table 3
Optimization of reaction conditions to maximize HMF yield.

Catalyst	Catalyst concentration (wt%)	Reaction time (h)	Reaction temperature (°C)	HMF yield (%)
ZrP-400	1	2	160	0.618
ZrP-400	1	4	160	1.213
ZrP-400	1	6	160	2.108
ZrP-400	2	2	160	0.706
ZrP-400	2	4	160	2.377
ZrP-400	2	6	160	4.328
ZrP-600	1	2	160	0.655
ZrP-600	1	4	160	2.158
ZrP-600	1	6	160	2.916
ZrP-600	2	2	160	0.804
ZrP-600	2	4	160	3.119
ZrP-600	2	6	160	3.526

The reusability of catalysts was also examined. After filtration of the reaction mixture, the residue which consisted of dark brown insoluble solid was dried at 103 °C for 12 h. The dried residue was then heated in a muffle furnace at 550 °C for 3 h to completely vaporize the volatile solids to get white powder of the ZrP catalyst. The recycled catalyst was used for next thermochemical reaction of FWB without any addition of fresh batch of catalyst. The results revealed that ZrP catalyst retained a good performance after being used 3 times with yield of HMF in the range of 3.7–4.8% (Data not shown). Therefore, it can be concluded that the catalyst is stable for repeated use.

The plausible reaction pathway of FWB conversion to HMF was also proposed and which involved three major steps i.e. (1) hydrolysis of FWB to glucose, (2) isomerization of glucose to fructose and (3) dehydration of fructose into HMF. FWB polysaccharides were hydrolyzed under hydrothermal conditions to produce glucose. Also, the acid site of catalysts weakens the glucosidic bonds of polysaccharides, thus producing monosaccharide i.e. glucose (Kuster, 1990; Aida et al., 2007; Wang et al., 2011; Brown, 2011). Further, through combined activity of protons released from water at high temperatures (Aida et al., 2007; Kuster, 1990) and acid sites presented on the surface of ZrP catalysts promotes the isomerization and dehydration reactions of glucose to HMF (Kuster, 1990; Aida et al., 2007; Wang et al., 2011; Brown, 2011; Yang et al., 2011a,b; Ordomsky et al., 2013).

3.4. Conceptual design and economic analysis

3.4.1. Conceptual process design

Fig. 3 shows an integrated process flow diagram of a HMF plant. The feed rate of the plant was determined by considering the annual FW generation in Singapore. The annual FW production in the year 2013 was 796,000 tons (NEA, 2012). It is assumed that that 60% of the generated FW would be processed in the plant and that the annual capacity of the plant would be 478,000 tons. When the annual production is converted into feed rate, it becomes 1309 tons/day. The feed is diluted to 50% using the recycle water from upstream and mixed with 25% ZrP catalysts. The feed is then pumped to the oil heater. On the way to the oil heater, the feed is heated to a higher temperature using recycled hot water from upstream. The feed is then heated to 160 °C by the oil heat and sent to the reactors. Three batch reactors are connected in series with a total residence time of 6 hours. The products from the reactor are cooled and pumped into a decanter V-101 to separate solid catalysts and hydro-char from the liquid phase. The catalysts were regenerated from the hydrochar by burning the catalysts and hydro-char mixture in H-102 heater to 550 °C. The extra heat generated from burning hydro-char could be used in the plant and reduce the cost of operation. However, in the present study this

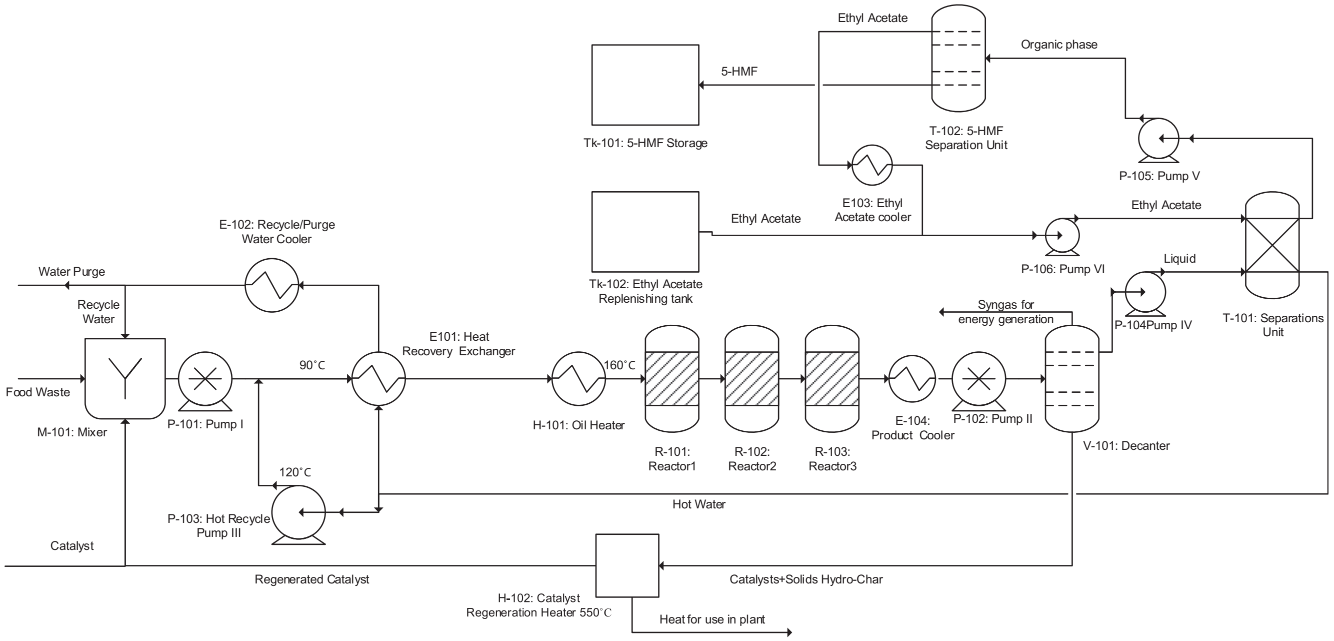

Fig. 3. Process flow diagram for the production of HMF from FWB.

option was not considered to ensure that cost of operation is not underestimated. The non-condensable gas, released from the decanter, mainly consists of carbon dioxide and methane, and can be used for energy generation within the plant. The liquid phase is sent to two separation units for upgrading, T-101 and T-102. In T-101, the organic phase is extracted from the liquid phase using ethyl acetate using 1:1 volume ratio. In T-102, the ethyl acetate solvent is vaporized to obtain purified HMF. The yield of HMF has been found to be 4% from experiments.

3.4.2. Preliminary economic analysis

3.4.2.1. Raw materials cost. The raw material cost is summarized in the Table 4. The raw materials cost account for FWB, ZrP catalyst and ethyl acetate solvent. FW was collected from various sites within Singapore. The collection cost of FW has been estimated to be US$ 60.79/ton (Kim et al., 2011). The collection cost includes the cost of acquiring FW from the sites, the transportation cost of FW, labor cost, etc. Material cost also includes the cost of catalysts and it contributes the major portion of the variable cost. The cost of ZrP is taken to be US $15 kg^{-1} from an online supplier. During experiments, the catalyst was regenerated 3 times and this has been used to calculate the annual catalyst cost. Ethyl acetate was also regenerated at the end of separation. Experimentally, ethyl acetate can be fully recovered, but to be pragmatic it is assumed that there is 10% loss in ethyl acetate per ton of HMF produced, which is 1912 tons per year. The market price of ethyl acetate is US$ 44.4 kg^{-1}.

3.4.2.2. Equipment cost. A detailed specification of the equipment is listed in Table S2 (see supplementary information). The sizing of the equipment has been taken from literature based on similar plants (Xing et al., 2011; Humbird et al., 2011). It should be noted that the cost is overestimated and not underestimated by considering the maximum size. When the sizing was different, the following scaling factor was used to find the appropriate price:

$$Cost_{new} = Cost_{base}\left(\frac{Capacity_{new}}{Capacity_{base}}\right)^{0.6} \tag{5}$$

Stainless steel has been considered as the preferred material of construction of most equipment as it is highly resistant to chemicals and rusting. The cost has been calculated using CAPCOST software.

3.4.2.3. Utilities cost. The utilities cost have been calculated for the powered equipment as shown in Table S3 (see supplementary information). The oil powered heater contributes the most to the utilities cost; about 60% of the total cost. It could be reduced if the syngas from the plant is recycled back and used as a heating source. The overall utility consumption of the plant can also be reduced by heat integration using optimization techniques.

3.4.2.4. Production cost. To determine annual production costs, Fixed Capital Investment (FCI) has to be estimated. It is the capital investment that can be depreciated i.e. all capital investment excluding land costs. Since the plant is a new development, FCI is equal to Grass Root cost and is given by:

$$FCI = 1.18\sum_i C_{BM,i} + 0.5\sum_i C_{BM,i} \tag{6}$$

Based on the raw materials cost, the utilities cost and the FCI, the total annual production cost has been calculated. The detailed calculation is shown in Table 5. The major cost is the cost of catalyst (ZrP) that accounts for about 80% of the total production cost.

3.4.2.5. Cash flow analysis. A discounted cash flow rate of return analysis method is performed to find out the minimum selling price (MSP) of HMF for a project of life span 20 years and construction period of 2 years. The investment is assumed to be made in two installments, 60% at the end of year 1 and the remaining 40% at the end of year 2. The calculation has been done by iterations in a Microsoft Excel spreadsheet. MSP is the selling price of the HMF that makes the net present value (NPV) of the process equal to zero, with a specified discounted cash flow rate of return over the overall plant life. The MSP has been found to be US$185.16 kg^{-1}. Fig. S6 (see supplementary information) shows the discounted cash flow over a period of 20 years for which the product is sold at the minimum price. Table S4 (see supplementary

Table 4
Table showing the raw material cost wand waste disposal cost. Annual plant capacity is 19120 ton of HMF.

Material name	Classification	Price ($/kg)	Flowrate (kg/h)	Annual cost ($)
Food waste	Raw material	0.06	54566.20	27,563,865
Bio-oil	Non-hazardous waste	0.04	45017.12	13,486,769
Hydro-char	Product	–	9549.09	–
Zirconium phosphate Catalyst	Raw material	15.00	9094.40	1,135,253,952
Ethyl acetate	Raw material	44.40	4092.47	1,512,154,569

information) shows the detailed calculation for the cash flow when product is sold at the minimum price.

In summary, preliminary analysis of production of HMF from FWB shows promising results in terms of economics. The minimum selling price has been determined to be US$185.16 kg^{-1}, which is significantly lower than current market price (US$ $8568 kg^{-1}). This MSP could be further reduced if hydrochar is considered as a saleable by-product; since the hydrochar obtained from decanter (83,650 tons annually) has high energy content (i.e. HHV value approximately 15.0 MJ kg^{-1}) and is also important feedstock for various energy and environmental applications.

3.5. Life cycle assessment

The evaluation of environmental impacts of the different stages of waste to energy/chemical conversion is extremely important for the purpose of protecting the community and natural environment (Khoo et al., 2010). Life cycle assessment (LCA) gives us the idea of material and energy flow per functional unit (kg ton^{-1}) of feed processed or product generated in a process. It is useful as it provides the impacts of different stages in the process (Gao et al., 2013). A preliminary LCA has been done to have an understanding of the environmental impacts of food waste to HMF and energy products conversion process.

Table 5
Summary of annual production calculation. Plant capacity: 19,120 ton HMF per year.

Economic options	
Cost of land	$1,250,000
Taxation rate	30%
Annual interest rate	10%
Salvage value	0
Working capital	$270,450,000
FCI_L (fixed capital investment)	$29,300,000
Total module factor	1.18
Grass roots factor	0.50
Economic information calculated from given information	
C_{RM} (raw materials costs)	$2,674,972,386
C_{UT} (cost of utilities)	$2,810,000
C_{WT} (waste treatment costs)	$13,486,769
C_{OL} (cost of operating labor)	$211,600
Factors used in calculation of cost of manufacturing (COM_d)	
$COM_d = 0.18 * FCIL + 2.76 * COL + 1.23 * (CUT + CWT + CRM)$	
Multiplying factor for FCIL	0.18
Multiplying factor for C_{OL}	2.76
Factors for C_{UT}, C_{WT}, and C_{RM}	1.23
COM_d	$3,316,119,077
Factors used in calculation of working capital	
Working capital = $A * C_{RM} + B * FCI_L + C * C_{OL}$	
A	0.10
B	0.10
C	0.10
Project life (years after startup)	20
Construction period	2
Distribution of fixed capital investment (must sum to one)	
End of year one	60%
End of year two	40%

3.5.1. Goal and scope

The goal of this life cycle analysis (LCA) is to have a preliminary understanding of the environmental impact of conversion of food waste into HMF. The functional unit of this study is 1 kg of HMF produced. The energy footprint is determined as total nonrenewable energy inputs per kg of HMF production (MJ kg^{-1} of HMF). These energy inputs include the electrical energy used in the process and also the indirect energy e.g. catalysts involved in the process chain. The carbon footprint is calculated based on the total direct and indirect greenhouse gas emission during the process. Three main greenhouse gases, CO_2, CH_4 and N_2O, are considered in terms of their CO_2 equivalent. The carbon footprint is expressed as grams of CO_2-eq kg^{-1} of HMF produced. It should be noted that the carbon trapped in food waste is not considered as carbon credit as this carbon will be emitted to the atmosphere after bio-fuel utilization in the form of CO_2. The scope of this LCA covers the conversion of 478,000 tons of food waste into HMF and other useful energy products. The process starts with collection of food waste followed by its hydrothermal conversion and separation of the products and co-products. Within the system boundary, the following assumptions are made:

- It is assumed that the transportation distance between the waste collection points to waste processing plants is all within 20 km. Transport emissions calculations will be based on this distance.
- The system boundary includes energy input in the form of diesel and electricity.
- All electricity requirements come from Singapore national grid power.
- Construction materials for development of plants and chemical input are not included in the system boundaries.
- Emission from hydrothermal conversion of food waste is considered negligible as the amount of gaseous products production is negligible.

3.5.2. Life cycle inventory

In life cycle inventory, the quantities of different resources required and emissions and waste generated per functional unit of the product are calculated. In these calculations, we consider energy as the main resource, the direct and indirect air emissions from the processes and energy requirements, and product output per functional unit. The electrical energy input to the conversion process and separation process is supplied by the Singapore national grid. The main emissions per KWh power supplied are shown in Table S5 (Gao et al., 2013).

From the preliminary studies done in this paper, as shown in Table S6 and Fig. S7, 97 MJ of energy is generated per kg of HMF produced from the process. Both hydro-char and bio-oil generated from this process are considered as co-products. When no co-products are considered, 87.5 MJ of energy is consumed per kg of HMF produced. In case of GHGs emissions, as shown in Table S7 and Fig. S8, the production of 1 kg of HMF via HTC process involved production of 16.59 g of CO_2 equivalent GHGs. The most rigorous stage which consumes the most electricity and emits maximum GHGs is the electrical heating process and the operation of the reactor to create high temperature and pressure conditions. LCA of HMF production from food waste does not exist in the literature and therefore could be compared with alternative pathway of HMF production. However, studies comparing different technologies for conversion of biomass into energy products or chemicals exist. Gao et al. (2013) compared anaerobic digestion with hydrothermal oxidation for production of bio-fuels from algal biomass. They concluded that the hydrothermal oxidation pathway requires less energy and smaller carbon footprints and therefore is environmentally more benign than anaerobic digestion. The amount of energy required to produce 1 kg of biofuel is reported to be around 34 MJ, which is comparable to the value obtained in this study. Khoo et al. (2010) performed LCA of different technologies for conversion of waste into useful energy products, but did not include HTC as this process was not in use in Singapore (Khoo et al., 2010). Gallardo (2011) studied LCA for the production of platform chemicals (similar to HMF) from lignocellusic biomass. In that study, the approximate GHGs emission for production of platform chemicals from lignocellusic biomass was 11.1–13.4 $kgCO_2$-eq (Gallardo, 2011), which is much higher than the preliminary results found in our study. The reason could be the starting biomass. The conversion process of lignocellusic biomass requires more severe operating conditions and for longer time, which significantly increases the energy consumption.

4. Conclusions

A novel thermochemical route was established for production of HMF from FWB. Usage of the heterogeneous catalyst, ZrP, has efficiently promoted the formation of HMF. Catalyst calcination temperature, catalyst dosage and reaction time have significant effects on the conversion of FW into HMF. ZrP catalyst retained the HMF conversion activity even after being used 3 times. A preliminary cost analysis has been done to find out the minimum selling price of HMF, which is US\$185.16 kg^{-1}. Overall, the present study suggests that thermochemical treatment is a promising approach for production of the value-added product, HMF, from FWB.

Acknowledgements

The authors are thankful to the National Environment Agency (NEA's) Environment Technology Research Programme (ETRP) Grant and National University of Singapore-Singapore for the financial support extended to this study. The authors are also thankful to Agency for Science, Technology and Research (A*STAR's) Institute of Materials Research and Engineering (IMRE), Singapore for technical assistance.

Appendix A. Supplementary data

Supplementary data associated with this article can be found, in the online version, at http://dx.doi.org/10.1016/j.biortech.2014.10.066.

References

Aida, T.M., Sato, Y., Watanabe, M., Tajima, K., Nonaka, T., Hattori, H., Arai, K., 2007. Dehydration of D-glucose in high temperature water at pressures up to 80 MPa. J. Supercrit. Fluids 40, 381–388.

Asghari, F.S., Yoshida, H., 2006. Acid-catalyzed production of 5-hydroxymethyl furfural from D-fructose in subcritical water. Ind. Eng. Chem. Res. 45, 2163–2173.

Bellezza, F., Cipiciani, A., Costantino, U., Marmottini, F., Quotadamo, M.A., 2006. Zirconium phosphate nanoparticles from water-in-oil microemulsions. Colloid Polym. Sci. 285, 19–25.

Benvenuti, F., Carlini, C., Patrono, P., Galletti, A.M.R., Sbrana, G., Massucci, M.A., Galli, P., 2000. Heterogeneous zirconium and titanium catalysts for the selective synthesis of 5-hydroxymethyl-2-furaldehyde from carbohydrates. Appl. Catal. A 193, 147–153.

Binder, J.B., Raines, R.T., 2010. Fermentable sugars by chemical hydrolysis of biomass. Proc. Natl. Acad. Sci. USA 107, 4516–4521.

Brown, R.C., 2011. Thermochemical Processing of Biomass: Conversion into Fuels, Chemicals and Power. John Wiley & Sons, Hoboken, NJ, c2011.

Carlini, C., Patrono, P., Galletti, A.M.R., Sbrana, G., 2004. Heterogeneous catalysts based on vanadyl phosphate for fructose dehydration to 5-hydroxymethyl-2-furaldehyde. Appl. Catal. A 275, 111–118.

Chang, S., Zhao, Z., Zheng, A., Li, X., Wang, X., Huang, Z., He, F., Li, H., 2013. Effect of hydrothermal pretreatment on properties of bio-oil produced from fast pyrolysis of eucalyptus wood in a fluidized bed reactor. Bioresour. Technol. 138, 321–328.

Corma, A., Iborra, S., Velty, A., 2007. Chemical routes for the transformation of biomass into chemicals. Chem. Rev. 107, 2411–2502.

Dashtban, M., Gilbert, A., Fatehi, P., 2014. Recent advancements in the production of hydroxymethylfurfural. RSC Adv. 4, 2037–2050.

Gallardo, M., 2011. Life Cycle Assessment of Platform Chemicals (phenolic compounds, solvent, soft and hard plastic precursors) from Fossil and Lignocellulosic Biomass Scenarios (Ph.D. thesis). Norwegian University of Science and Technology, Norway.

Gao, X., Yu, Y., Wu, H., 2013. Life cycle energy and carbon footprints of microalgal biodiesel production in western australia: a comparison of byproducts utilization strategies. ACS Sustainable Chem. Eng. 1, 1371–1380.

Huang, Y.B., Fu, Y., 2013. Hydrolysis of cellulose to glucose by solid acid catalysts. Green Chem. 15, 1095–1111.

Humbird, D., Davis, R., Tao, L., Kinchin, C., Hsu, D., Aden, A., Schoen, P., Lukas, J., Olthof, B., Worley, M., Sexton, D., Dudgeon, D., 2011. Process design and economics for biochemical conversion of lignocellulosic biomass to ethanol. Technical Report. National Renewable Energy Laboratory (NREL) USA.

Khoo, H.K., Lim, T.Z., Tan, R.B., 2010. Food waste conversion options in Singapore: Environmental impacts based on an LCA perspective. Sci. Total Environ. 408, 1367–1373.

Kim, M.H., Song, Y.E., Song, H.B., Kim, J.W., Hwang, S.J., 2011. Evaluation of food waste disposal options by LCC analysis from the perspective of global warming: Jungnang case, South Korea. Waste Manage. 31, 2112–2120.

Kuster, B.F.M., 1990. 5-Hydroxymethylfurfural (HMF). A Review focussing on its manufacture. Starch 42, 314–321.

Lin, H., Strull, J., Liu, Y., Karmiol, Z., Plank, K., Miller, G., Guo, Z., Yang, L., 2012. High yield production of levulinic acid by catalytic partial oxidation of cellulose in aqueous media. Energy Environ. Sci. 5, 9773–9777.

Lin, S.K.C., Pfaltzgraff, L.A., Herrero-Davila, L., Mubofu, E.B., Solhy, A., Clark, J.H., Koutinas, A., Kopsahelis, N., Stamatelatou, K., Dickson, F., Thankappan, S., Zahouily, M., Brocklesby, R., Luque, R., 2013. Food waste as a valuable resource for the production of chemicals, materials and fuels. Current situation and global perspective. Energy Environ. Sci. 6, 426–464.

NEA Waste Statistics and Overall Recycling, 2013. <http://app2.nea.gov.sg/energy-waste/waste-management/waste-statistics-and-overall-recycling>.

Ordomsky, V.V., van der Schaaf, J., Schouten, J.C., Nijhuis, T.A., 2013. Glucose dehydration to 5-hydroxymethylfurfural in a biphasic system over solid acid foams. ChemSusChem 6, 1697–1707.

Parshetti, G.K., Chowdhury, S., Balasubramanian, R., 2014. Hydrothermal conversion of urban food waste to chars for removal of textile dyes from contaminated waters. Bioresour. Technol. 161, 310–319.

Pfaltzgraff, L.A., De Bruyn, M., Cooper, E.C., Budarin, V., Clark, J.H., 2013. Food waste biomass: a resource for high-value chemicals. Green Chem. 15, 307–314.

Puziy, A.M., Poddubnaya, O.I., Ziatdinov, A.M., 2006. On the chemical structure of phosphorus compounds in phosphoric acid-activated carbon. Appl. Surf. Sci. 252, 8036–8038.

Sheldon, R.A., 2014. Green and sustainable manufacture of chemicals from biomass: state of the art. Green Chem. 16, 950–963.

Wang, P., Yu, H., Zhan, S., Wang, S., 2011. Catalytic hydrolysis of lignocellulosic biomass into 5-hydroxymethylfurfural in ionic liquid. Bioresour. Technol. 102, 4179–4183.

Watanabe, M., Aizawa, Y., Iida, T., Nishimura, R., Inomata, H., 2005. Catalytic glucose and fructose conversions with TiO_2 and ZrO_2 in water at 473 K: relationship between reactivity and acid–base property determined by TPD measurement. Appl. Catal. A 295, 150–156.

Weingarten, R., Tompsett, G.A., Conner Jr, W.C., Huber, G.W., 2011. Design of solid acid catalysts for aqueous-phase dehydration of carbohydrates: the role of Lewis and Brønsted acid sites. J. Catal. 279, 174–182.

Weingarten, R., Kim, Y.T., Tompsett, G.A., FernÃ¡ndez, A., Han, K.S., Hagaman, E.W., Conner Jr., W.C., Dumesic, J.A., Huber, G.W., 2013. Conversion of glucose into levulinic acid with solid metal (IV) phosphate catalysts. J. Catal. 304, 123–134.

Xiao, S., Liu, B., Wang, Y., Fang, Z., Zhang, Z., 2014. Efficient conversion of cellulose into biofuel precursor 5-hydroxymethylfurfural in dimethyl sulfoxide–ionic liquid mixtures. Bioresour. Technol. 151, 361–366.

Xing, R., Qi, W., Huber, G.W., 2011. Production of furfural and carboxylic acids from wastes aqueous hemicelluloses solutions from the pulp and paper and cellulosic ethanol industries. Energy Environ. Sci. 4, 2193–2205.

Yan, L., Laskar, D.D., Lee, S.J., Yang, B., 2013. Aqueous phase catalytic conversion of agarose to 5-hydroxymethylfurfural by metal chlorides. RSC Adv. 3, 24090–24098.

Yang, F., Liu, Q., Bai, X., Du, Y., 2011a. Conversion of biomass into 5-hydroxymethylfurfural using solid acid catalyst. Bioresour. Technol. 102, 3424–3429.

Yang, F., Liu, Q., Yue, M., Bai, X., Du, Y., 2011b. Tantalum compounds as heterogeneous catalysts for saccharide dehydration to 5-hydroxymethylfurfural. Chem. Commun. 47, 4469–4471.

Yuan, Z.Y., Ren, T.Z., Azioune, A., Pireaux, J.J., Su, B.L., 2005. Marvelous self-assembly of hierarchically nanostructured porous zirconium phosphate solid acids with high thermal stability. Catal. Today 105, 647–654.